THE 23RD CHESAPEAKE SAILING YACHT SYMPOSIUM
ANNAPOLIS, MARYLAND, MARCH 2019

Experimental measurement and simplified prediction of T-foil performance for monohull dinghies

Sandy Day, University of Strathclyde, Glasgow Scotland
Margot Cocard, University of Strathclyde, Glasgow Scotland
Moritz Troll, University of Strathclyde, Glasgow Scotland

Exocet Moth - Photo © Katie Hughes

ABSTRACT

The rise in interest in large foiling yachts, such as those in the America's Cup, has spurred a corresponding interest in foiling applications in monohull sailing dinghies, both for boats designed specifically for foiling, and through retro-fit foil kits. The present study considers the assessment of foil systems for such boats, and specifically the prediction of the necessary foil performance of T-foils with flaps.

The main lifting foil for a moth dinghy with flap was tested at full-scale in a towing tank at a range of speeds, trim angles and flap angles, and immersions, to measure vertical and lift and drag. Results are then compared with two simplified models typical of those utilized in Velocity Prediction Programs for preliminary design. The first model uses section lift and drag data obtained using the well-known XFOIL code allied to a simple correction for 3D effects while the second model deploys a numerical lifting line theory in conjunction with section data.

A number of practical conclusions are drawn regarding the set-up and sailing of foiling dinghies with flapped T-foils. Results show that whilst the simple and rapid models typically used in basic VPPs may not accurately represent the relationships between angle of attack / flap angle with lift and drag, the predicted relation between lift and drag is reasonably accurate in most cases.

Notation

AR	Aspect Ratio (geometric)
b	Foil span
c	Foil chord
e	Oswald Efficiency Factor
C_D	Drag Coefficient
C_{Di}	Induced Drag Coefficient
C_{Dw}	Wave Drag Coefficient
C_{Dj}	Junction Drag Coefficient
C_{Dws}	Wave and Spray Drag Coefficient
C_L	Lift Coefficient
C_{Lh}	Lift Coefficient at immersion h
DA	Drag Area
D_j	Junction Drag
D_{ws}	Wave and Spray Drag
h	Immersion
LA	Lift Area
Re	Reynolds Number
t	Thickness
TR	Taper Ratio
V	Speed
α	Angle of attack (horizontal foil)
Λ	Sweep Angle
ρ	Density
φ	Flap Angle (horizontal foil)

Other symbols are defined as required in the text.

INTRODUCTION

Foiling dinghies have become popular in the last decade, led by developments in the International Moth. Foiling boats won races in the Moth world championships as long ago as 2000, and the Moth world championship was won for the first time in a foiling boat in 2005. The foil set-up for the Moth is restricted by the class rules, so that foils must exit the hull below the static waterline. This has led to the universal adoption in Moths of a foil system comprising two T-foils mounted on the centerline. This layout is therefore quite different to the foil configurations often seen on larger foiling catamarans, typically employing a pair of L- or J-foils as the main lifting surfaces along with T-foil rudders.

In the Moth system, the main horizontal foil is rigidly attached to the vertical (centreboard), although on some boats it is possible to adjust the rake of the vertical slightly to account for different wind conditions by moving the top of the foil fore and aft. The vertical is typically raked forward at around 7° to reduce the risk of ventilation. The ride height is controlled via a trailing edge flap on the main horizontal foil, which is activated through a mechanical linkage by a wand mounted on the bow of the boat, or, in more boats, on a short bowsprit. Within this mechanical system, the relationship between the angular movement of wand and flap is adjusted using a gearing system, whilst the neutral position of the flap relative to the wand position can be adjusted via a ride height or bias adjuster.

The lifting foil on the rudder is rigidly attached to the vertical, and the rudder lift is normally controlled by moving the top of the rudder assembly fore and aft using a screwed rod turned via a twist grip in the tiller extension, thus raking the rudder vertical and changing the angle of attack of the lifting foil. This is generally adjusted relatively infrequently to account for changes in wind speed, or changes from upwind to downwind sailing.

Modern Moths are capable of speeds in excess of 30 knots, and foil tacking is normal at the higher level of the racing fleet. While the boats vary in design, competitive boats are relatively expensive, with most boats beings 100% carbon fibre, and with increasing use of high modulus carbon in foils. Even so, the boats can be fragile with all-up sailing weight around 35kg. In this context, a number of production one-design foiling boats have been developed in recent years using T-foil systems based on standardized, and, in some cases, lower cost, implementations of the Moth system. These include monohulls such as the *Waszp*, *Skeeta* and *Onefly*,

catamarans with twin T-foil systems such as the *Whisper* and *Stunt 9* and trimarans such as the *F101*.

Most of the development of foiling Moths has been achieved via full-scale trials of equipment, although increased interest in foiling boats is encouraging developments in modelling tools. However, whilst a number of studies have been published examining performance prediction for T-foil boats in general and moths in particular (e.g. Findlay and Turnock (2008)), Bögle *et al.* (2010), Mackenzie (2014)), relatively few recent studies have focussed on experimental measurements of flapped T-foils.

Historical studies of fully-submerged hydrofoils (e.g. Ramsen & Vaughan (1955), Wadlin *et al.* (1955) Ripken (1961)) were typically aimed at design of foils for large powered vessels. As such, the foil geometries are typically very different, and generally did not employ flaps, at least in the test programs. Binns (2017) has carried out a series of detailed measurements investigating ventilation around T-foils, both in the towing tank, and from a powered catamaran, following an earlier study (Binns *et al.* 2008) on an unflapped T-foil broadly similar to a Moth foil, although with lower aspect ratio.

Beaver & Zseleczky (2009) carried out a highly detailed study of the fluid flow around a Moth Dinghy, including tank testing of the hull, several main foil, and rudder foil, and aerodynamic testing for the hull and sailor; Andersson *et al.* (2017) executed a comprehensive set of hydro-and aerodynamic studies in the successful design, build, and sailing of the "Foiling Optimist", including tank test studies of hull with and without foils and wind tunnel testing of the sails. These studies formed the starting point for the present work.

The aim of the present work was to develop a test rig suitable for testing flapped T-foils in a towing tank and to use the test rig to develop a data set for validation of computational analysis of foil phenomena. In the longer term it is intended to use the data to validate high-fidelity predictions of complex phenomena associate with the foils, including effects of yaw and heel, and foil tip immersion; however, the present study is confined to upright foils with no yaw over a range of angles of attack and flap angles. Since CFD studies may not always be well-suited to early stage design, and velocity prediction, a second aim is to investigate the accuracy of some relatively simple models which may be deployed in velocity prediction programs for foiling boats.

TANK TESTING

The towing tank study was conducted in two stages. A preliminary stage took place in early 2018 to commission and troubleshoot the test set-up, whilst the main test campaign took place in late 2018, as the first part of a study into foil performance.

T-foil tested

The foil utilized for the present tests was chosen for pragmatic reasons, largely related to availability. The foil is from a rather old "*Bladerider*" design of International Moth (originally designed around 2006) owned by one of the authors. However, it appears to be similar to the foil described as "Vendor 1" tested by Beaver and Zseleczky (2008). The foil is regarded as slow by modern Moth standards, with the horizontal in particular being thicker, less stiff, and more fragile than modern competitive Moth foils. The key dimensions of the foil are shown in Table 1.

Table 1 - Main dimensions of foil

Horizontal	Span	0.988 m
	Chord at root (extrapolated due to bulb)	0.125 m
	Chord at 90% span	0.045 m
	Mean Chord (area / span)	0.095 m
	Thickness / Chord	12.8%
	Camber / Chord	3.1%
Vertical	Span (from bottom of hull)	1.0 m
	Chord at root (bottom of hull)	0.118 m
	Chord at tip	0.1135 m
	Thickness / Chord	14.5%

The foil was mass-produced using carbon skins and a foam core, unlike modern foils which are generally solid carbon fibre (and now increasingly often high modulus carbon fibre). However, for the purposes of the present study, it is sufficiently similar to a contemporary Moth foil to allow the test rig to be validated and useful results to be gained for comparison with numerical predictions. The foil is also more comparable than a state-of-art

Moth foil to some of the rather more basic foils utilised in production foiling boats. The foil is shown in Figure 1.

The flap comprises very close to 35% of the chord for the vast majority of the foil; it is attached using a hinge consisting of a bead of a flexible jointing compound on the upper surface. A squashed bulb in the center of the horizontal allows adequate reinforcement of the joint between the horizontal and vertical foils. The vertical foil is installed in the boat with forward rake, intended to reduce the incidence of ventilation, and the angle of attack of the horizontal foil is mounted to reflect that.

Figure 1 -T-foil tested

The precise geometry of the foil is not publicly available. However, the manufacturers published CAD drawings of the geometry of a series of jigs which could be used at a range of span-wise locations for holding the flap at the neutral angle whilst refurbishing the hinge. By scaling the jig drawings, it could be seen that the sections were close to geometrically similar along the span. The largest section had the highest number of points, and was used to generate an offset table for the horizontal section. This is shown in Figure 2. The vertical section appeared to match very closely with a NACA 66012 section scaled to 14.5% thickness. In the numerical study no attempt was made to model the foil bulb; instead the profile was extrapolated to the centreline.

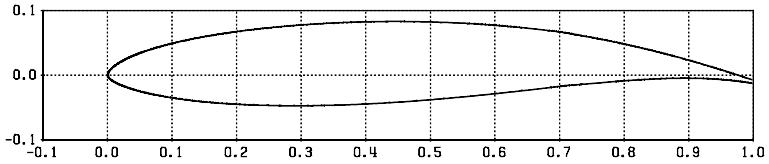

Figure 2 - Horizontal Foil Cross section

Equally some other details which may have some impact on the hydrodynamics were ignored in the numerical modelling – in particular the gap in the lower surface of the horizontal which allows the flap to rotate in the positive (downward) sense, and the cut-out at the rear lower part of the vertical which allows the flap to rotate in the negative (upward) sense.

Test Rig and instrumentation

Test were carried out in the towing tank of the Kelvin Hydrodynamics Laboratory in Glasgow, Scotland. The tank is 76 m long, 4.6 m wide, and 2.5 m deep, with a water depth for these tests of 2.1 m. The towing carriage has a maximum speed of just over 4.6 m/s. For the present tests a bespoke test rig was constructed which was attached to the vertical member of the standard towing post.

The vertical component of the foil was mounted in a frame which could be pivoted in rake (or pitch/trim) relative to the fixed part of the test rig to allow the angle of attack of the horizontal foil to be varied. The vertical position of the foil could be easily adjusted within the frame to vary immersion. The fixed part of the test rig was mounted on two tri-axial load cells. These load cells were more sensitive in the X and Y directions than in the Z direction, and were therefore oriented so that X and Y corresponded to the vertical lift and drag forces. Each mount had a bearing releasing moments in the pitch axis, whilst the upper mount was also fitted with a low

friction slide to release the vertical force. The test rig support could thus be regarded as equivalent to a classical simply-supported beam mounted vertically. The flap on the foil was actuated via a screw mechanism acting on the bell-crank at the top of the vertical foil which in turn activates the flap control rod running through the vertical foil. A pointer was installed to indicate the flap angle at the top. The test rig is shown in Figure 3.

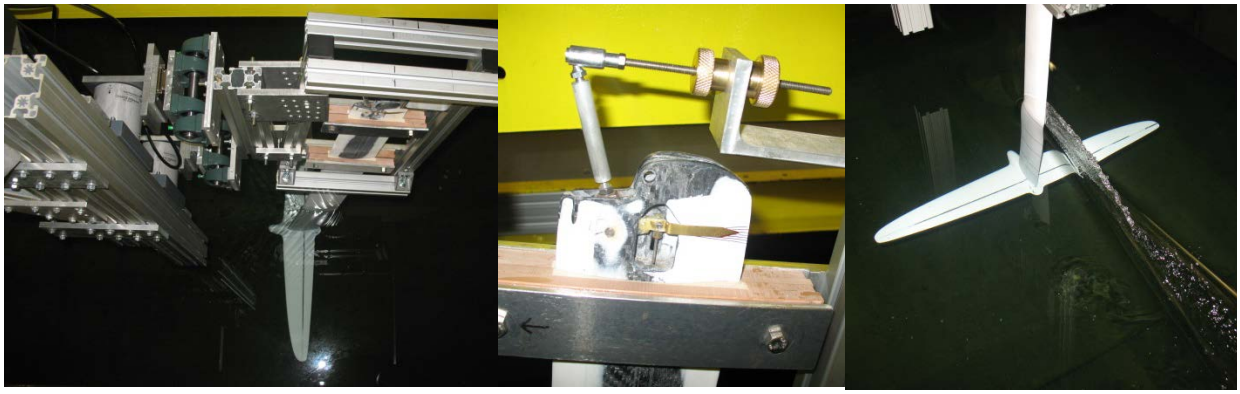

Figure 3 Towing Tank Test Rig

The load cells were calibrated individually in all three directions, and the cross-coupling between load in each direction and the measured load in the other two directions was determined separately for each cell, with particular attention paid to the coupling between lift and drag. The test rig was then assembled with the vertical in place and the rig performance was verified by applying horizontal loads at various vertical locations and vertical loads at various horizontal locations corresponding to typical test conditions.

It should be noted that whilst the rotation of the foil assembly and of the flap can be measured accurately relative to the starting position, it is difficult to be completely precise about the zero position of both the angle of attack of the horizontal and of the flap angle. This is discussed later in comparison with numerical results. The uncertainty in the main foil arises because it is common practice to use shims to adjust the angle of attack of the horizontal relative to the vertical prior to bonding the foils together permanently, so every foil assembly is likely to be slightly different.

A further issue with the flap angle is that it was observed in some cases that the pointer indicating the flap angle was moving under load. This was presumed to be due to the relatively slender push rod (2.5 mm stainless steel) which controls the flap bending inside the vertical. Once this had been realized, the pointer was videoed during the tests so that the value indicated by the pointer could be determined under load after the tests. This was predominantly noticeable in cases at the highest speeds with large angle of attack and large flap angle, which are less relevant to normal sailing conditions for the Moth – for example, in some cases, the pointer moved more than 2° at the highest speeds with angle of attack of 6°. For these reasons, where possible, these angles are not used as independent variables in presenting the results.

This highlights the practical issues involved in precise control of the flap in the boat under sailing conditions for which the speeds (and loads) can be much higher. In recent years, Moths have moved away from thin steel rods towards the use of much larger diameter carbon tubes for the pushrod components running between the wand and the top of the vertical, but the lack of space inside the thin trailing edge of the vertical foil presents a challenge in stiffening this component.

The tank testing procedure was extremely straightforward once the rig was installed; the immersion, flap angle, and angle of attack were set, and the carriage accelerated up to speed, whilst measuring the load in the load cells and the speed of the carriage. In the first version of the rig it had proved difficult to alter the angle of attack; however, after a re-design, this was easily altered, so once the range of speeds was complete for a given angle of attack / flap angle combination, the angle of attack was altered. Once all angles of attack were complete the flap angle was then changed.

The majority of the tests were carried out at a submergence of 457 mm (18”), corresponding to 4.8 × mean foil chord. This is rather deep for a moth foil in sailing condition, but was chosen for several reasons. The maximum carriage speed in the Kelvin Lab is 4.5 m/s which is not far above take-off speed for a Moth (typically around 3.5 m/s boat speed for this boat), at which point the boat would be flying quite low, and so a relatively deep

submergence of the foil is appropriate in that sense. This depth also matches some data from the previous study by Beaver & Zseleczky (2008), allowing a comparison to be made. Finally, it reduces the impact of wave making & free surface effects on the foil, giving a good baseline condition.

A range of speeds from 0.5 m/s to 4.5 m/s (mean chord Re 0.4×10^5 to 3.6×10^5) with a step of 0.25 m/s was explored for the case of angle of attack $\alpha = 0°$ and flap angle $\varphi = 0°$. Whilst the lower speeds are of no practical relevance for foil sailing, they add some insight into the hydrodynamics of the foil. With a flap angle of zero, the angle of attack was varied from 0° to 6° with a step of 1° at speed increments of 0.5 m/s. For the remainder of the tests, angles of attack from 0° to 6° and flap angles of –6° to +6° with steps of 2° were utilized with speeds varying from 2.0 m/s to 4.5 m/s and a step of 0.5 m/s. This speed range corresponds to a mean chord Reynolds Number range 1.6×10^5 to 3.6×10^5. In order to explore the effects of free surface proximity, a second, shorter, series of tests was carried out with a submergence of 100 mm. A total of nearly 400 tests were carried out, including a substantial number of repeats.

One question which would benefit from further study is the impact of turbulence on the flow over the foil, and in particular, in the nature of the laminar-turbulent transition. The level of turbulence experienced by a foil advancing in a towing tank into essentially still water may well be lower than that in the water in which a foiling boat is sailing when wind speeds are high enough to foil, and especially in wavy conditions, although this is dependent on the waiting time between test runs. Furthermore, it is likely that vibration may play a part – on the towing carriage there is always some small mechanical vibration, whilst in the real boat the foils may "sing" due to hydroelastic effects at higher speeds. In the present tests no attempt was made to measure background turbulence in the water or on the foil.

Results

Results are presented in terms of lift and drag forces (N) and lift and drag areas (equivalent to product of lift and drag coefficient and the relevant reference areas), defined as:

$$LA = Lift/\left(\frac{1}{2}\rho V^2\right)$$

$$DA = Drag/\left(\frac{1}{2}\rho V^2\right)$$

The use of lift and drag areas was adopted in order to avoid any requirement to decompose forces between horizontal and vertical foils with different chords, thicknesses and areas. Variation of lift and drag, and the corresponding areas with speed are shown in Figure 4 and Figure 5.

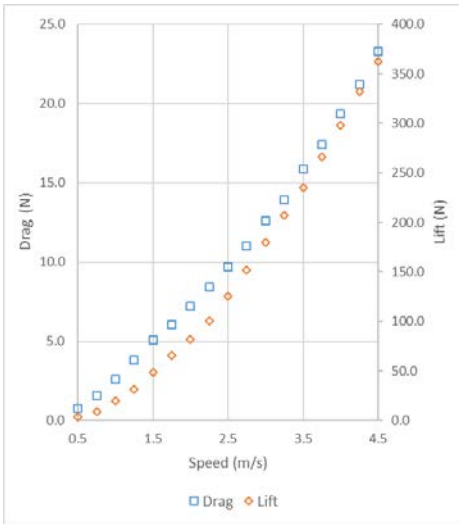

Figure 4 Variation of lift and drag with speed: $\alpha = 0$, $\varphi = 0$

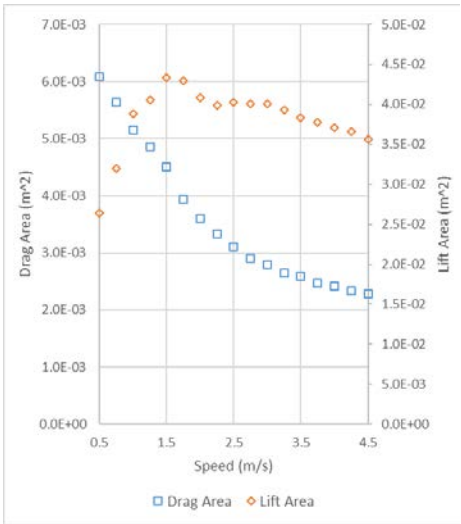

Figure 5 Variation of lift and drag areas with speed: $\alpha = 0$, $\varphi = 0$

The drag area reduces as speed and Reynolds Number increase, as might be expected, whilst the lift area peaks at 1.5 m/s, corresponding to a mean chord Reynolds number of 1.2×10^5, and then reduces slowly. The variation

of lift and drag area with angle of attack with the flap at zero degrees over a range of speeds is shown in Figure 6. As expected the lift slope is slightly less than linear as angle of attack increases, whilst the drag shows slightly more subtle variations; both lift and drag areas reduce with speed and Reynolds Number, as expected from Figure 5.

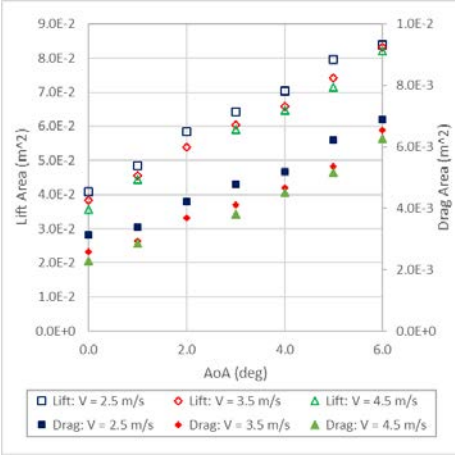

Figure 6 Variation of lift and drag areas with angle of attack: $\varphi = 0$

The variation of foil performance as flap angle and angle of attack were varied is shown for a selection of speeds in Figure 7. Each set of seven points corresponds to a single angle of attack with a range of flap angles from –6° to +6° at 2° intervals. In this case, the data is presented as drag area versus lift area squared, in order to eliminate flap angle as an independent variable, since the flap angles varied under load in some cases as discussed in the previous section. This is arguably the most important curve in terms of velocity prediction.

It is interesting to note that the curves for angles of attack from 0° to 4° almost collapse onto a single line. This has the practical implication of suggesting that the performance of the foil in sailing condition is not especially sensitive to the precise set up of the horizontal relative to the vertical within a relatively broad range of angles of attack. The only real exception to this is for the rather extreme angle of attack of 6°, which yields higher drag. It is also apparent that the six-degree angle of attack curve shows a small dip in the middle, particularly at the lowest speed. This point corresponds to the condition of zero flap angle. A similar, although less pronounced, feature can be observed in the other curves.

The variation of foil performance between speeds of 2.0 m/s and 4.0 m/s is shown in Figure 8. These speeds correspond to mean-chord-based Reynolds Number range of 1.6×10^5 to 3.2×10^5. As expected from Figure 5, both lift and drag area reduce as the speed increases, but the drop in drag outweighs the drop in lift, and hence the foil can be seen to perform more efficiently at the higher speed. The change is most pronounced at the lower speeds (between 2 m/s to 3 m/s); it can be seen from Figure 7 that the differences between 3.5 m/s to 4.5 m/s are much smaller than those shown in Figure 8.

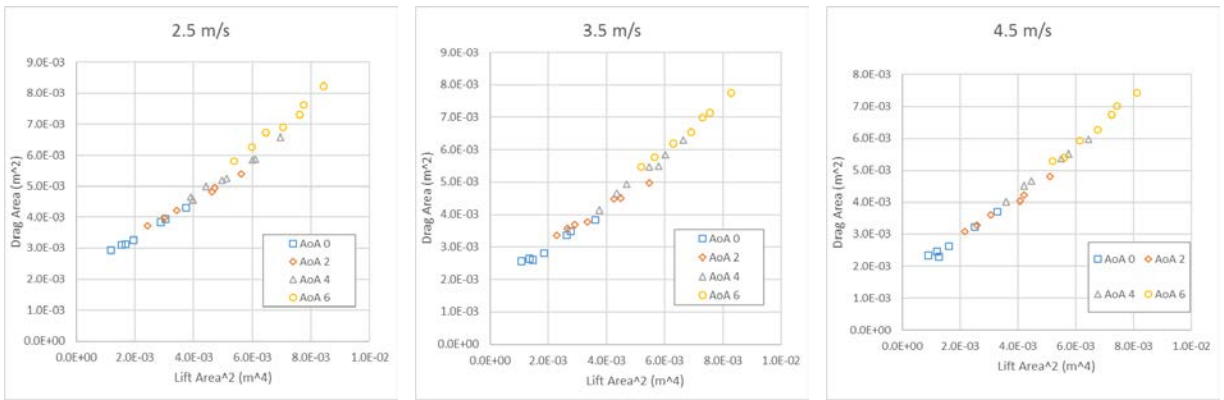

Figure 7 Variation of lift and drag areas with angle of attack and flap angle

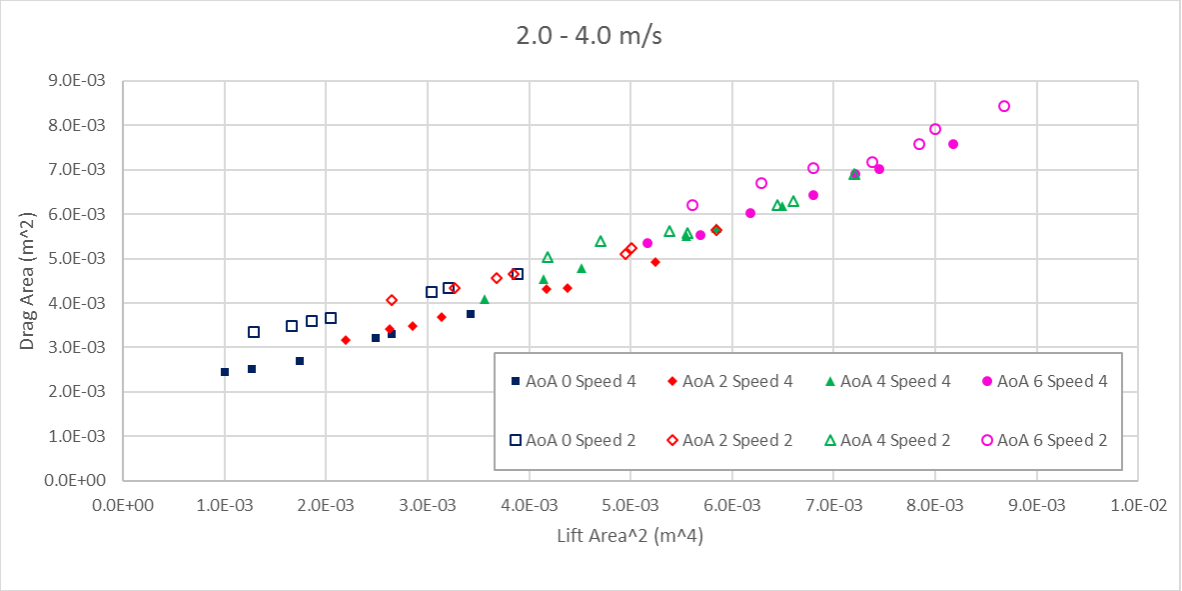

Figure 8 Sensitivity of Lift and Drag Areas to speed

Figure 9 shows the variation of lift and drag as immersion is reduced from 457 mm (4.8 × mean chord) to 100 mm (1.05 × mean chord) for an angle of attack of zero degrees and flap angles of zero and six degrees. It can be seen that the variation is rather small when the flap angle is neutral, but that both lift and drag drop substantially as submergence is reduced in the condition with greater flap angle, when lift is greater. It should be noted that this is not expected to be a realistic condition, as it is highly unlikely that a Moth would be set up to have such a large flap angle at a ride height high enough to yield this low immersion.

As immersion reduces, less of the vertical foil is immersed, leading to a drop in viscous drag; at the same time the wave drag of the horizontal foil may be expected to increase as the foil approaches the surface. Moth sailors typically sail high in flat water for maximum speed, so it may be expected that there is a net gain in performance in realistic sailing conditions as immersion reduces.

The small increase in lift at the highest speed with zero flap angle is less expected, although this may be within uncertainty due to the flap angle. It is worth mentioning that for the shallower immersion for which the waves generated are larger, there may be an effect of depth Froude Number at the higher speeds, further complicating an already complex issue.

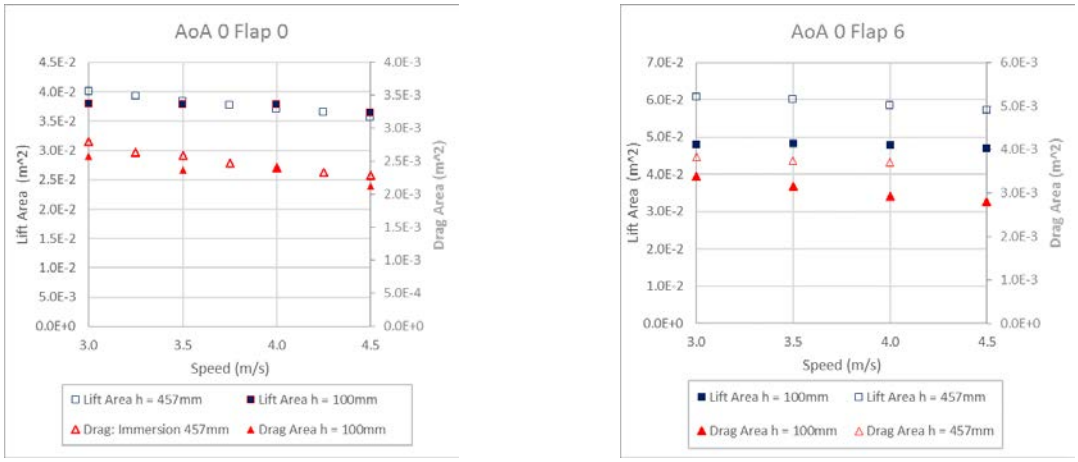

Figure 9 Sensitivity of Lift and Drag Areas to immersion: α = 0°, φ = 0° & α = 0°, φ = 6°

Since shallow immersion is likely to be related to higher speeds, the fastest tests are of most practical interest here. The comparison for all cases tested at 4.5 m/s is shown in Figure 10. The solid markers show the points at the 100 mm immersion, with flap angles –6°, 0° and 6°. The open markers show the points at 457 mm

immersion, with flap angles from –6° to +6° at 2° steps. It can be clearly seen that there is a cross-over point in this plot. At low lift conditions, with small angles of attack and small flap angle (as would be the case for a Moth flying high) the performance is improved by reducing the immersion, with slightly less drag generated for the same amount of lift. Here it is expected that the reduction in drag of the vertical is greater than the increase in resistance of the horizontal due to free surface proximity.

Conversely in higher lift conditions, the shallow immersion gives reduced performance, with more drag at the same level of lift. As mentioned before these conditions are highly unlikely to occur in practice (at least intentionally). Hence this plot illustrates why flying high is generally likely to be fast in a Moth.

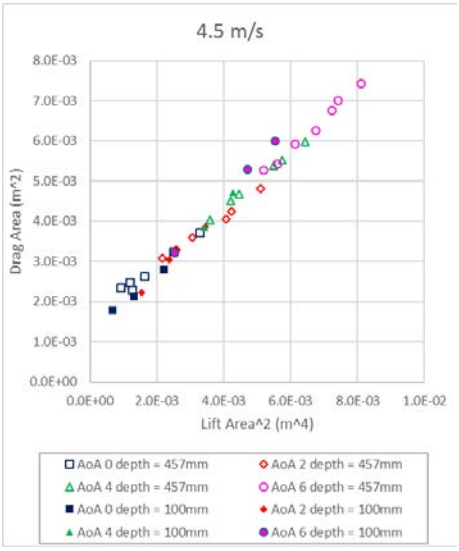

Figure 10 Sensitivity of Lift and Drag Areas to immersion: V = 4.5 m/s

SIMPLIFIED MODELLING OF T-FOIL

A high fidelity model of the behaviour of the foils is likely to require the use of a CFD code with free surface capability; this is undoubtedly a challenging task due to the complex geometry of the foil details such as the flap and hinge, the bulb, and the cut-outs, leading to a need for a dense mesh; at the same time, hydrodynamic features such as the thin sheet of water running up the vertical, the spray from the vertical foil, and the wave pattern generated (see Figure 3) will also present challenges in terms of domain size and mesh density. This is likely to lead to very substantial implications for computer resource in terms of numbers of cores and run time required, even for a small number of cases.

Whilst CFD results should in principle lead to the highest possible fidelity of prediction, one of the goals of the present study was to examine how well the hydrodynamic behaviour of the foils could be predicted by relatively simple models, particularly those which can be run very rapidly on a simple PC, and may be deployed in a VPP. To this end two highly simplified approaches have been deployed, both of which are many orders of magnitude faster than a CFD model.

Simplified Model 1

The simplest model deployed here for the T-foil broadly follows the approach described by Andersson *et al.* (2017), which was successfully deployed in the design of the "Foiling Optimist". The section lift and drag characteristics of the horizontal foil section are analyzed over a range of speeds, angles of attack and flap angles, using the well-known publicly-available XFOIL 6.99 code (Drela (2013)), employing a coupled panel method and integral boundary layer approach. The same code was used to determine section drag coefficients for the vertical foil.

The 3D lift coefficient was then obtained using the simple equation based on lifting line with elliptical lift distribution:

(1) $$C_L^{3D} = C_L^{2D} / \left(1 + \frac{2}{AR}\right)$$

Here C_L^{2D} is the section lift coefficient obtained from XFOIL at a nominal Reynolds Number based on mean chord, and AR is the geometric aspect ratio. The lift is then obtained in the usual manner. The profile drag is obtained from the XFOIL section drag coefficient (again at a nominal Reynolds Number) applied to the area of the foil. Induced drag is obtained from the lifting line result for an elliptical foil:

(2) $$C_{Di} = C_L^2/\pi AR$$

Following Beaver and Zseleczky (2009), the coefficient of wave drag for the horizontal foil based on planform area was taken from Hoerner (1965) (section 11-26) as:

(3) $$C_{Dw} = C_L^2 \frac{h}{c} \frac{C_D}{C_{Lh}^2}$$

where h is the submergence, and Beaver and Zseleczky (2009) give $\frac{C_D}{C_{Lh}^2} = 0.25$.

Wave and spray drag for the vertical foil are estimated using empirical values for drag coefficient found in Hoerner (1965) (section 10-13) as:

(4) $$D_{ws} = \frac{1}{2}\rho V^2 C_{Dws} t^2$$

Here C_{Dws} is the combined wave and spray drag coefficient based on strut thickness t, given as 0.54. Finally the drag due to flow around the junction between main foil and vertical is estimated based on a drag coefficient based on thickness using a further equation from Hoerner (1965) (section 8-11):

(5) $$D_j = \frac{1}{2}\rho V^2 C_{Dj} t^2 \quad \text{and} \quad C_{Dj} = 17\left(\frac{\bar{t}}{c}\right)^2 - 0.05$$

Here $\bar{t}$ is the mean thickness of the horizontal and vertical foils. This approach may be very easily implemented in a simple environment such as MS Excel once the section lift and drag coefficients from have been obtained from XFOIL.

In the present implementation, for each foil section, XFOIL was run for 3126 cases comprising 6 Reynolds numbers ranging from 1.0×10^5 to 1.0×10^6, 13 angles of attack from –4° to 8°, and 17 flap angles, from –8° to 8°. In all cases free transition was utilised with a value of the XFOIL parameter *Ncrit* set to 4, corresponding to a turbulence level of around 0.6%. An example data set for $Re = 4 \times 10^5$ is shown in Figure 11.

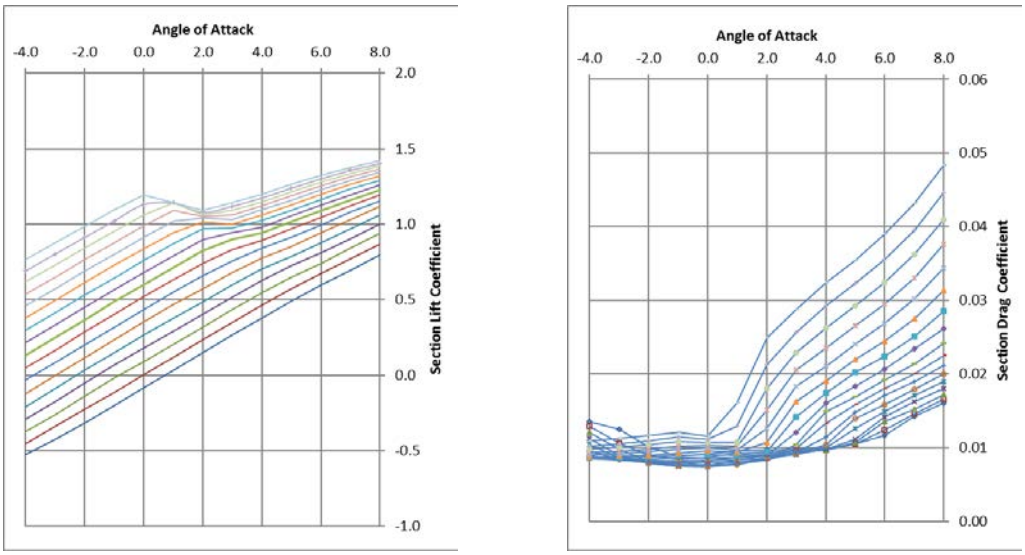

Figure 11 XFOIL Section lift and drag coefficients for Bladerider foil: $Re = 4 \times 10^5$, $\varphi = -8^\circ$ to 8°

As discussed previously, the level of turbulence in both sailing and tank test conditions is somewhat uncertain, and laminar-turbulent transition may well not occur in the tank test or sailing conditions via the "natural"

transition modelled here in XFOIL. Further investigation of turbulence levels and transition models are planned for future studies.

The section lift and drag data generated was stored in an Excel sheet; cubic spline surface interpolation was then used to find the coefficients for a given Reynolds number and angle of attack for each of the flap angles, and then cubic spline interpolation was used again to find the value for the given flap angle.

Simplified Model 2

Whilst a model very similar to that described above had clearly been used with great success in design of the foiling optimist, it was of interest to see to what extent it could be improved without dramatically increasing the requirement for computational resource. An approach was developed using a numerical implementation of a lifting line method in MS Excel, using a total of 21 span-wise stations across the main foil.

The lifting line approach utilised data from XFOIL to estimate a linearized lift slope and zero-lift angle for the foil section at the given flap angle, based on the mean chord Reynolds Number. The lifting line solution was used to calculate local angles of attack at each span-wise station and induced drag coefficient. The local angles of attack were then used in turn in conjunction with the local Reynolds Numbers and the XFOIL section drag coefficients to estimate profile drag. The profile drag of the vertical foil was estimated using the XFOIL data as in the first model described above. A number of corrections were then explored for the various lift and drag values obtained in this manner.

The effect of the free surface was included using an approach described in Daskovsky (2000), deploying an approximation to 3D biplane theory. In this approach, the free surface influences both the lift and the drag of the foil. The lift coefficient is multiplied by the factor:

(6) $$(1 + 2/AR)/(1 + 2K(1 + \sigma)/AR)$$

Here

(7) $$K = \frac{16(h/c)^2+1}{16(h/c)^2+2} \quad \text{and} \quad \sigma = 1/(1 + 12\,h/b)$$

where h is the submergence, c is the chord (taken here as mean chord) and b is the foil span. With the same approach, the induced drag coefficient is multiplied by the factor $(1 + \sigma)$. This approach is shown to yield similar results to the model proposed by Wadlin (1955), based on a horseshoe vortex near a free surface, although Wadlin's model is rather more complex to implement. This approach is based on infinite Froude Number. For finite Froude numbers wave-making effects should also be considered. Daskovsky suggests the use of the approximate relationship:

(8) $$C_{Dw} = \frac{C_L^2}{2F_c^2}\exp(-(2h/c)^2/F_c^2)$$

Here F_c is the Froude Number based on chord. This was found to give broadly similar results to the approach suggested in Vladimirov (1955).

The effect of the vertical foil on the lift from a fully-submerged foil was modelled according to a recommendation in Gibbs & Cox (1954) for strut interference. The lift and induced drag coefficients are multiplied by the factors:

(9) $$C_{Lstrut} = C_L/(1 + \gamma)$$

$$C_{Di\,strut} = (1 + \gamma)^2 C_{Di}$$

where $\gamma = 0.8t/b$ for a central strut. Further study of this effect is found in Ripken (1961), although the data in this study is presented in a manner which is not easy to use.

The effect of the wave and spray around the vertical foil is calculated utilising data from Coffee and McKann (1953), who suggest that the wave and spray drag be estimated from:

(10) $$D_{ws} = \frac{1}{2}\rho V^2 C_{Dws} ct$$

The published data for moderate chord Froude numbers and a 12% thick section, shows that C_{Dws} is approximately 0.0275. It should be noted that the reference area in this equation is different from that of equation (4). Similar results were obtained by Ramsen and Vaughan (1955).

In the current Moth flap, the hinge is made of flexible sealant, whilst in more modern foils it is often made with Kevlar cloth impregnated with flexible epoxy. As a result, the flow from the lower surface cannot flow through the hinge to the upper surface. The hinge of the flap is flush with the upper surface, and the foil thus has a substantial cut-out on the lower surface designed to allow the flap to deflect down. This clearly impacts the flow on the lower surface. A substantial body of published data exists for drag due to flaps for aircraft (e.g. Wenzinger and Harris (1939)). It should be noted that in the published studies of cases for which the geometry is broadly similar to present foil, the flaps are typically slotted, and fluid may flow through the gap between the main foil and flap which may lead to different behaviour from the Moth foil. Nonetheless the correction suggested by Wenzinger and Harris (1939) was adopted here – this adds a drag coefficient increment of 0.0012 for lift coefficients below 0.6 and then linearly increases to 0.0022 for lift coefficient of 1.0.

Finally, the effect of the bulb was acknowledged in a crude manner by scaling the viscous drag coefficient according to the ratio of the planform area including the bulb to the planform area without the bulb. This added approximately 3% to the area. No attempt was made to correct for the cut-out in the vertical foil, and the bulb.

COMPARISON WITH EXPERIMENT DATA

The comparison of the two models with the experiment data of Figure 4 for zero angle of attack and zero flap angle is shown in Figure 12 below.

Here the solid points are the laboratory data; the curves labelled “2D model” are calculated using model 1 from section 0 while the curves labelled “LL” are calculated using model 2 of section 0. Since there was a small degree of uncertainty related to the precise value of the zero of the angle of attack of the main foil, curves are presented for both 0° and -0.5°.

Both models over-predict lift, with relatively small differences between them; model 2 is slightly better than model 1. Model 1 predicts drag reasonably well at an assumed angle of attack of 0°, whilst model 2 predicts drag better at assumed angle of attack of -0.5°. For reliable VPP predictions, however, the relationship between angle of attack/ flap angle and drag or lift is arguably less important than the relationship between drag and lift. Furthermore, the model must also perform well at different flap angles and different immersions.

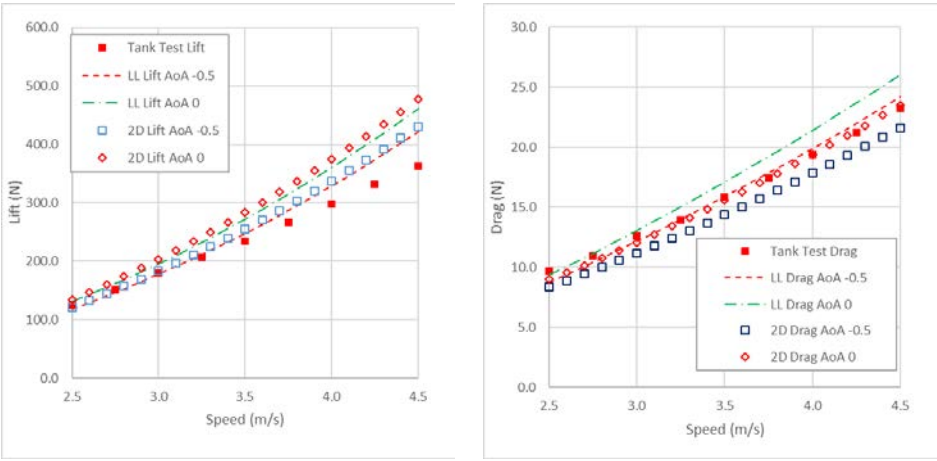

Figure 12 Comparison of approximate models with test data for varying speed: $\alpha = 0$, $\varphi = 0$

Figure 13 shows data for a range of flap angles and angles of attack at a speed of 4.0 m/s. Each curve corresponds to a fixed angle of attack and consists of points representing seven flap angles from –6° to 6° in 2° steps. In these plots the data is again plotted as Drag Area versus Lift Area squared to reduce the effect of the uncertainty of flap angle and angle of attack in the measured data.

It can be seen from these curve that the general trend of the relationship between drag and lift predicted by the very simple model 1 matches fairly well with experiment data, even if the values of lift and drag at a given flap

angle are relatively inaccurate. The slightly more sophisticated model 2 generally performs better than model 1 in virtually all cases, although the agreement is noticeably less good for higher angles of attack, which may affect prediction of take-off speed.

This data suggests that where the simple model is implemented in a VPP model the hydrodynamic drag of the foil will be broadly correct for a fixed lift value for the boat when flying (related to the weight), but that the angle of attack and/or flap angle required to achieve that lift value will be incorrect. However, use of this approach would lead to errors if the VPP predicted large positive or negative flap angles where values of lift may be predicted which are not achievable in practice; this might affect take-off speed prediction.

If the VPP uses a model representing the mechanical linkage between the wand and the flap, relating flying height to flap angle, then use of data from these models could lead to the VPP predicting the boat flying at a height which is different to that achieved in practice, with the corollary that the foil immersion will then be incorrect. This will then have a secondary effect on the drag. However, whilst sailing a modern Moth, it is common to adjust both the zero position of the flap relative to the zero position of the wand (using a “ride height” or “bias” adjuster) and the ratio of flap angle movement to wand angle movement (using a “gearing” adjuster) and, so this model is likely to be somewhat arbitrary in any case.

The effect of submergence is shown in Figure 14, in which the data is presented for the tested immersion of 100 mm, or 1.05 × mean chord at an angle of attack of 0° and flap angles of 0° and 6°. With flap angle of 0° there is relatively little change from the deeper submersion case, as seen in Figure 9.

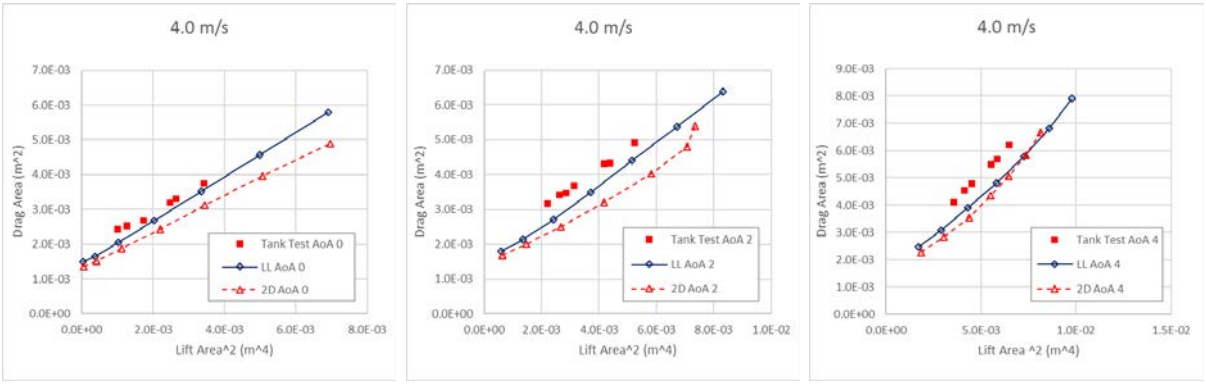

Figure 13 Comparison of approximate models with Test Data: *V* = 4.0 m/s

The lifting line model performs fairly well, especially at the higher speeds, predicting drag quite accurately, and slightly under-predicting lift, while the simpler model over predicts both lift and drag. At the higher flap angle neither approach works well in this respect; the simpler approach predicts drag quite accurately while dramatically over estimating lift, while model 2 underestimates both lift and drag for large flap angles, as seen in Figure 12.

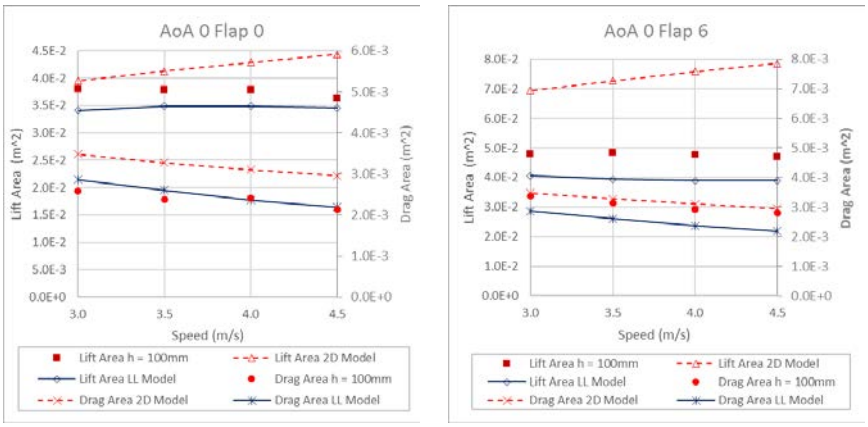

Figure 14 Comparison of approximate models with Test Data: Lift & Drag v. Speed: h = 100 mm

As mentioned previously, however, for performance prediction the most important issue is the relationship

between drag and lift. This is shown for the two models at the highest speed in Figure 15. In a manner which may be compared to the discussion of the results of Figure 13, it can be seen the relationship between drag and lift is predicted reasonably well in both models, even though the relationship between angle of attack and drag and lift is not predicted so well for large flap angles. This is especially true in the cases of most practical relevance to small immersion; i.e. those with low angles of attack and small flap angles.

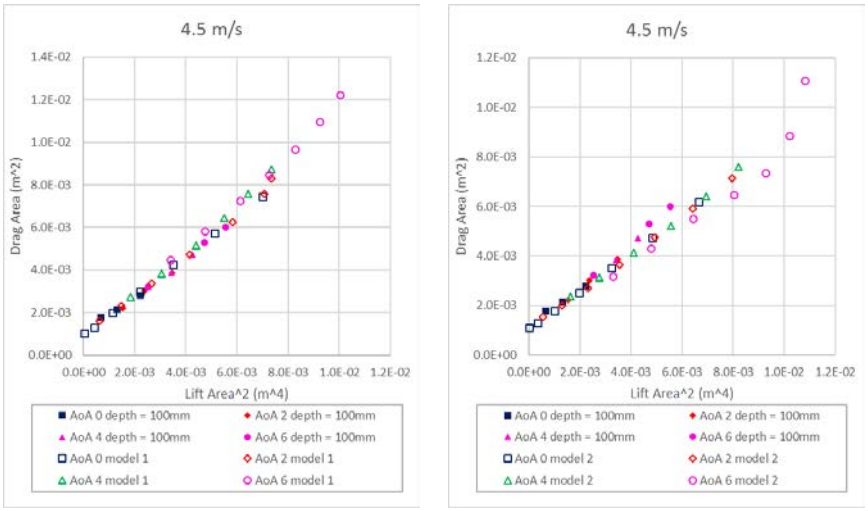

Figure 15 Comparison of approximate models with Test Data: Lift v Drag, h = 100 mm

It should be noted that many combinations of models and corrections could be assembled from the range of semi-empirical models and simplified theoretical models deployed here or in other studies. For example, model 1 could usefully utilize approximate corrections for lift and drag related to planform efficiency (Oswald Factor) such as those suggested by Niţă & Scholz (2012) as

$$e = 1/\left(1 + f\left(TR - \Delta TR\right) AR\right) \tag{11}$$

with:

$$\Delta TR = -0.357 + 0.45\exp\left(0.0375\Lambda\right)$$

and

$$f\left(TR\right) = 0.0524TR^4 - 0.1500TR^3 + 0.1659TR^2 - 0.0706TR + 0.0119$$

This yields a value of e = 0.97 for the current foil. This will lead to improved predictions in some cases.

In general, however, it must be said that further systematic test data is highly desirable for identifying the best simple corrections, especially in terms of free surface effects, in order to identify with confidence the most reliable approach. It should also be noted that it is extremely likely that such simple models will never be able to capture all of the complex flow physics, and that more sophisticated models will be required for high-fidelity predictions.

Nonetheless it can be seen that both of the models examined are broadly successful in predicting the performance of a flapped t-foil; the lifting line approach required a little more effort, but can still easily be set up in an Excel spreadsheet. The simple model can very easily be built into a VPP; whilst the calculation of the lifting line approach may be a little slow for implementation within a VPP, the foil performance may easily be tabulated prior to running the VPP in a manner similar to that used for the XFOIL data in the present calculation. The VPP can then interpolate data for foil performance whilst solving the equations of equilibrium.

CONCLUSIONS

A test rig for evaluating the performance of a flapped T-foil has been designed, built and tested, using a foil from an International Moth dinghy.

Tests were carried out over a range of angles of attack, and flap angles which might be encountered in sailing a Moth; speeds were restricted by the tank capability to a maximum of 4.5 m/s, which is at the lower end of foiling speeds for a Moth.

As well as providing a benchmark data set for analysis of flapped T-foils, a number of practical conclusions may be drawn from the test which can inform future work.

At high angles of attack and large flap angles, when high lift coefficients may be developed, it was found that the control rod fixing the flap angle was bending. From the view the model test this lead to some uncertainty in the flap angle (although it was measured by video during the test). From the view of the sailor, this will lead to less precise control. However, a design solution is not obvious.

When plotting drag against lift for a variety of combinations of angles of attack and flap angle, it is seen that the curves at moderate angles of attack collapse close to a single line, with only very large positive flap angles yielding higher drag for a given lift. This suggests that the performance of the boat will not be especially sensitive to the precise angle fixing the main foil relative to the vertical foil.

The effect of foil immersion has been examined for a small number of cases. In low lift conditions, (small angle of attack and flap angle) which would be expected for Moths flying high, it can be seen that drag is reduced at a given lift compared to deeper immersion. It is presumed that this effect results from the loss of drag on the vertical foil outweighing the gain in drag and loss of lift on the horizontal foil.

This result is expected from observation of Moth sailors who generally fly as high as possible in a given set of conditions. However, for high lift conditions (large angle of attack and flap angle), the reverse is true, and the foil has more drag at the lower immersion. This condition is not of great practical relevance, since Moths flying high will not have large flap angles under normal conditions.

Two simple models have been examined for predicting the performance of the T-foil. Both are sufficiently simple to be implemented on a spreadsheet. The first model uses 2D section data in conjunction with simple empirical equations and some approximate results from lifting line theory; the second model is based on a solution of lifting line theory deploying 2D section data.

It is found that both models predict the relationships between drag and lift fairly well over the range of conditions tested, although the drag is somewhat underestimated in high-lift conditions. The model based on the lifting line generally out-performs the simple model by a small margin. However, both could be regarded as suitable for implementation in a VPP at a level of fidelity appropriate for early-stage preliminary design studies. However, more test data is needed for further validation, especially with regard to some of the more complex flow phenomena, and it is very likely that more sophisticated models will be required to capture all features of the flow physics

Acknowledgements

The authors would like to acknowledge the technical staff of the Kelvin Hydrodynamics Lab: Steven Black and Bill Wright for building the test rig and Dr Saishuai Dai and Grant Dunning for support in testing. We also acknowledge Thomas King and Dr Weichao Shi for carrying out the preliminary study used to troubleshoot the test rig design.

References

Andersson, A., Barreng, A., Bohnsack, E., Larsson, L., Lundin, L. Sahlberg R., Werner E., Finnsgård C., Persson A., Brown, M. and McVeagh, J., “The Foiling Optimist”, Proceedings 4th International Conference on Innovation in High Performance Sailing Yachts (Innov’sail), Lorient, France 2017

Beaver, B., Zseleczky, J., “Full Scale Measurements on a Hydrofoil International Moth”, Chesapeake Sailing Yacht Symposium, Annapolis, USA, 2009

Binns, JR Brandner, PA and Plouhinec, J, “The effect of heel angle and free-surface proximity on the performance and strut wake of a moth sailing dingy rudder t-foil” Proceedings 3rd High Performance Yacht Design Conference Auckland, 2008

Binns, JR, Ashworth Briggs, A, Fleming, A, Duffy, J, Haase, M and Kermarec, M, Unlocking hydrofoil hydrodynamics with experimental results, Proceedings 4th International Conference on Innovation in High Performance Sailing Yachts (Innov’sail), Lorient, France 2017

Bögle, C., Hochkirch, K., Hansen, H., Tampier-Brockhaus, G, “Evaluation of the Performance of a Hydro-Foiled Moth by Stability and Force Balance Criteria”, 31. Symposium Yachtbau und Yachtenwurf, Hamburg, Germany November 2010

Coffee, C. W. and McKann, R. E. “Hydrodynamic Drag of 12- and 21- percent Thick Surface Piercing Struts” NACA Technical Note 3092. 1953

Daskovsky, M, “The hydrofoil in surface proximity, theory and experiment”, Ocean Engineering, Volume 27, Issue 10, Pages 1129-1159, October 2000

Drela M., “XFOIL”, http://web.mit.edu/drela/Public/web/xfoil/, 2013

Hoerner, S., “Fluid Dynamic Drag”, Hoerner Fluid Dynamics, Albuquerque, USA, 1965

Findlay, M. W., Turnock, S. R. “Investigating sailing styles and boat set-up on the performance of a hydrofoiling Moth dinghy”, Proc. 20th International HISWA Symposium on Yacht Design and Construction, Amsterdam, Netherlands, 2008

Gibbs and Cox inc. “Hydrofoil Handbook Vol II: Hydrodynamic Characteristics of Components” ONR Hydrofoil Research Project, 1954

Mackenzie, J.R. “Can a Flapless Hydrofoil Provide a Realistic Alternative To a Standard Moth Foil With a Flap?” HISWA Symposium Amsterdam, Netherlands, 2014

Niţă, M. and Scholz, D. “Estimating the Oswald Factor from Basic Aircraft Geometrical Parameters” Deutscher Luft- und Raumfahrtkongress 2012

Ramsen, J. A. and Vaughan, V. L. “Hydrodynamic Tares and Interference Effects for a 12-Percent Thick Surface-Piercing Strut and an Aspect-Ratio-0.25 Lifting Surface. NACA Technical Note 3420, 1955

Ripken, J. F. “Interference effects of a strut on the lift and drag of a hydrofoil” Bureau of Ships project No SF 013 02 01, Task 1702, ONR Contract Nonr-710(39), 1961

Vladimirov, A. N. “Approximate Hydrodynamic Design of a Finite Span Hydrofoil” NACA Technical Memorandum 1341, 1955

Wadlin, K.L., Shuford, C.L., Jr., McGehee, J.R., “A theoretical and experimental investigation of the lift and drag characteristics of hydrofoils at subcritical and supercritical speeds”. NACA Report No. 1232. 1955

Wenzinger, C.J. and Harris, T. A. “Wind-tunnel investigation of an NACA 23012 airfoil with various arrangements of slotted flaps” NACA Report 664, 1939